Accuracy and Stability Improvements of Integral Equation Models Using the Partial Element Equivalent Circuit (PEEC) Approach

Jan E. Garrett, *Member, IEEE,* Albert E. Ruehli, *Fellow, IEEE,* and Clayton R. Paul, *Fellow, IEEE*

***Abstract*—The partial element equivalent circuit (PEEC) technique is a formulation which transforms an electric field integral equation (EFIE) into a full-wave equivalent circuit solution. In this paper, improvements are made to the PEEC model through the development of a refined method of computing both the partial inductances as well as the coefficients of potential. The method does not increase the number of unknowns. In addition, damping is added to the PEEC model in order to further reduce nonphysical resonances which may occur above the useful frequency range. The observations and solutions presented in this paper are especially important for time domain solvers. The effectiveness of the method is illustrated with several examples.**

***Index Terms*— Circuit analysis, integral equations, radiation, partial elements, scattering.**

I. Introduction

THE demand for electromagnetic (EM) modeling has increased considerably in the last few years. For example, the modeling of electronic systems for electromagnetic compatibility (EMC) [1] and electrical interconnect and packages (EIP) require efficient solution techniques for large problems which can accommodate a wide range of geometries. These modeling tools should be applicable to both radiation as well as scattering problems. An example of a scattering or incident field problem for electronic systems is the radiated electromagnetic susceptibility to radio and television signals. These mixed EM and circuits problems are very challenging for electromagnetic formulations both in terms of problem size and complexity.

The partial element equivalent circuit (PEEC) approach [2] is particularly useful for the modeling of electromagnetic problems, which include very large scale integration (VLSI) circuits or circuit elements. Also, more insight can be gained into the solution details using this approach. In the work presented in this paper, we introduce several improvements of the PEEC model, which increase both the accuracy and the stability for time-domain applications. The PEEC method is based on a circuit interpretation of an electric field integral equation (EFIE) full-wave formulation. Results similar to a method of moments (MoM) formulation [3], [4] can be obtained using a circuit-solver program. The basic PEEC formulation has recently been extended to include incident fields or scattering [5], dielectrics [6], lossy dielectrics [7], and the use of the modified nodal analysis (MNA) as well as the modified loop analysis (MLA) formulation in [8].

The applicability of the PEEC model to both time- and frequency-domain problems is very useful. Very often, additional insight can be gained from the analysis of a problem in both domains. Simple PEEC models which do not involve delays can be applied to both domains using a conventional circuit solver like Spice [9] or ASTAP [10]. In this paper, we are restricting ourselves to the frequency-domain analysis. However, we are using the frequency results for the time-domain stability analysis, which, to date, has not been solved for general problems. Instabilities for the time-domain integral equation formulations for EM problems have been observed by many authors where some of the earlier work is given in [11]–[14]. Many different techniques have been suggested to overcome these instabilities. In particular, [15] uses a conjugate gradient method, [16] uses a filtering technique, and [17] uses the matrix pencil technique to eliminate late time instabilities. While all of these techniques help eliminate some of stability problems for specific cases, some sources of instabilities remain.

In this work, we are using a different approach. In a recent paper on stability [18], it was observed that the discretization of the continuous time EFIE leads to an unstable discrete system since the model may have poles in the right half plane. We know from circuit theory that the PEEC models *without* delays are passive and stable. Hence, it is evident that the instabilities are caused by the delays between the partial inductances and the coefficients of potential. Many test have shown that well implemented MoM and PEEC formulations with delays do give very simular frequency responses in the region of interest where the cells are chosen to be sufficiently small such that the cell size is at least 20 cells/λ. Note that impedance computations, like the ones we consider in this paper, do require more cells for an accurate solution than do radiation problems. Throughout this paper, we call the lower frequency range corresponding up to wavelength where all cells are of a size $\geq$20 cells/λ the *active* frequency range. Also, we call the upper bound of the active region $f_{\max}$. Higher frequencies correspond to a much smaller number of cells than 20 cells/λ. We call this frequency range the *extended* frequency range with an upper bound f_e. The motivation

Manuscript received October 15, 1996; revised October 16, 1997.

J. E. Garrett is with IBM AS/400 Division, Rochester, MN, 55901 USA.

A. E. Ruehli is with the T. J. Watson Research Center, IBM Research Division, Yorktown Heights, NY 10598 USA.

C. R. Paul is with Mercer University, Macon, GA 31207 USA.

Publisher Item Identifier S 0018-926X(98)09735-X.

for computations in the extended frequency range is the fact that we observed a complex resonance behavior of the models in this range. This may be totally irrelevant for a straightforward frequency analysis, but is extremely important for other applications like the time-domain analysis and for model reduction techniques.

In this paper, we try to understand and to eliminate the undesirable resonance behavior in the *extended* frequency range. We start to formulate our approach with two observations.

Observation 1: The discretized models exhibit seemingly random resonances in the extended frequency range, which may correspond to frequencies that considerably exceed the 20 cells/λ limit. These resonances or poles are a strong function of the cell divisions of the discretization. The input port impedance may exhibit a negative real part at these resonances.

This behavior can lead to very poor frequency responses since some of these resonances or poles have a very large amplitudes or residues. This may lead to problems for model reduction based techniques like [19] and [17] and also for above mentioned late time instability problem.

One of the issues we had to resolve was how we could observe these "bad" or false resonances. The analytical and numerical eigenvalue computation method in the recent paper [18] can only be applied to very small problems. Attempts are in progress to compute the eigenvalues for larger problems [20]. Here, we resort to another approach for the observation of the unstable behavior of the model. We know from circuit theory that given a passive circuit, the input impedance must be positive real, where a positive real function is defined in [21] as follows.

Definition 1: A function $F(s)$ of the complex variable s is said to be positive real if $F(s)$ is real when s is real, $\mathrm{Re}[F(s)] \geq 0$ when $\mathrm{Re}[s] = 0$, and $\mathrm{Re}[F(s)] > 0$ when $\mathrm{Re}[s] > 0$.

We monitor the real part of the input impedance of a PEEC model $\mathrm{Re}[Z(s)] \geq 0$ for frequencies $s = j\omega \geq 0$ to observe if the terminal impedance violates this condition. Also, this is a relatively simple test to perform and we found that it gives us very useful insights into stability problem as will be evident from the results section. One of our aims is to maintain the real part of the input impedance to be positive up to as high a frequency as possible. Instabilities at very high frequencies are much easier to contain by using an implicit time integration method, which has numerical damping like the backward Euler method [22]. This was also confirmed by an experimental time domain solver [23].

Observation 2: Rynne [12] observed that the period τ of the frequency of the undesirable oscillation in time-domain solutions is in some cases related to the time step h as $f = \frac{1}{2h}$.

We can assume that the time-integration method creates a very high frequency noise at this frequency. As an example, a time step of $h = 0.005$ ns is typical for the type of problems of interest. This corresponds to a frequency of 100 GHz according to the observation. We found that the frequency of oscillation may be spread over a wide range of frequencies into several hundred GHz for a model which may have the usual 20 cells/λ at a frequency of $f_{\max} = 20$ GHz! This led us to the study of the PEEC model for frequencies up to $50 f_{\max}$ or 1000 GHz. Some of the frequencies of oscillation in the time domain are clearly not related by the above time step relation. The examples in the results show that the spurious resonance can occur at rather arbitrary frequencies which are a strong function of the discretization. Fundamentally, it is possible to eliminate the spurious resonances by increasing the number of cells. However, this is a very undesirable approach since the number of unknowns and solution time increases drastically with the number of cells. The stabilization technique should not increase the number of unknowns. Further, to stabilize the time-domain solution, the same technique must be applicable to the time-domain as well as to the frequency-domain formulations.

The usual retarded or delayed PEEC model with losses is denoted as and (L_p, P, R, τ) PEEC model. However, since we exclusively consider models with delay, we simply call them PEEC. Also, for notational convenience, we call a model with the stabilization a +PEEC or a R+PEEC model. In Section II, we derive the PEEC models for both partial inductance and for coefficients of potential beginning with the EFIE. Then, in Section III, we derive the PEEC model improvements (+PEEC) and (R+PEEC). In Section IV, results are presented.

II. Short Derivation of the PEEC Model

Again, we are only interested in PEEC models which involve retardation or delays τ between the elements. The purpose of this section is to briefly introduce an appropriate integral equation formulation for such a PEEC model. Then, we define both the partial inductance and the coefficient of potential terms that are important for the PEEC improvements in the next section.

A. Integral Equation Formulation

The electric field in free-space at a conductor can be written for the nondielectric case as

$$\frac{\bar{J}(\bar{r})}{\sigma} + j\omega\mu \int_{v'} G(\bar{r}, \bar{r}')\bar{J}(\bar{r}')\, dv' + \frac{\nabla}{\epsilon_0} \int_{v'} G(\bar{r}, \bar{r}') q(r')\, dv' = \bar{E}(\bar{r}) \tag{1}$$

where $\bar{J}$ is the current density in the conductor, q is the charge density, and G is the free-space Green's function

$$G(\bar{r}, \bar{r}') = \frac{e^{-j\beta R}}{4\pi R} \tag{2}$$

where R is given by $R = |\bar{r} - \bar{r}'|$.

The unknown quantities J and q are assumed constant over a cell. The geometry is discretized into small enough cells so that this assumption is valid. The cell size restriction due to $f_{\max}$ already leads to a basic discretization. A further refinement of the cells may be necessary where conductors are closely spaced. In the PEEC formulation, both q and J are unknowns and are related by the continuity equation $\nabla \cdot \bar{J} + j\omega q = 0$. The continuity equation is enforced in the circuit solution at each node in the form of Kirchoff's current law.

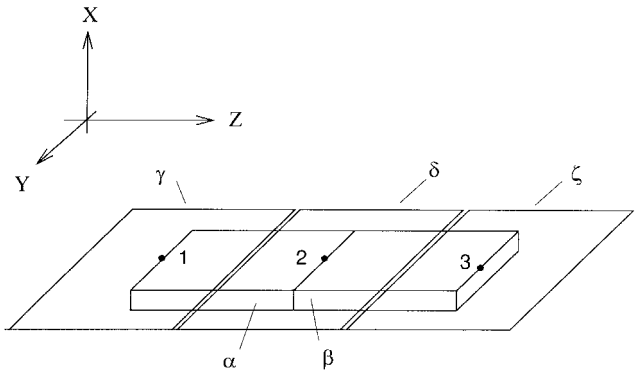

Fig. 1. Two-cell conductor example.

The vector quantities are discretized into orthogonal coordinates as $\bar{J} = J_x\hat{x} + J_y\hat{y} + J_z\hat{z}$. Substituting this relationship into (1) will result in a set of three equations that are identical in form but differ in spatial directions x, y, z. As an example, consider the current for the conductor shown in Fig. 1 that has been discretized into two volume cells α and β and three surface cells γ, δ, ζ.

Substitution of the z component of the current into the integral equation for a perfect electric conductor results in

$$0 = \hat{n} \times \left(j\omega\mu \int_{v_{\alpha'}} G(\bar{r},\bar{r}')\bar{J}_z(\bar{r}')\, dv_{\alpha'} + j\omega\mu \int_{v_{\beta'}} G(\bar{r},\bar{r}')\bar{J}_z(\bar{r}')\, dv_{\beta'} + \frac{1}{\epsilon_0}\frac{\partial}{\partial z}\int_{S_{\gamma'}} G(\bar{r},\bar{r}')q(r')\, dS_{\gamma'} + \frac{1}{\epsilon_0}\frac{\partial}{\partial z}\int_{S_{\delta'}} G(\bar{r},\bar{r}')q(r')\, dS_{\delta'} + \frac{1}{\epsilon_0}\frac{\partial}{\partial z}\int_{S_{\zeta'}} G(\bar{r},\bar{r}')q(r')\, dS_{\zeta'} \right)_{\text{on PEC}}. \quad (3)$$

The basis and testing functions are selected corresponding to the two types of unknowns: the current density $\bar{J}$ and charge q. Each unknown is expanded into a series of pulse-basis functions with an unknown amplitude. Pulse functions are also selected for the testing functions for the Galerkin formulation utilized in PEEC. The cell-to-cell coupling is defined with respect to cell α in Fig. 1 by integrating each term of the integral equation (3) over the volume v_α of conductor cell α in the following manner:

$$\frac{1}{a_\alpha}\int_{v_\alpha} f(\bar{r})\, dv = \frac{1}{a_\alpha}\int_{a_\alpha}\int_{l_\alpha} f(\bar{r})\, da\, dl \quad (4)$$

where v_α is the volume of the conductor cell α, a_α is the cross section of the cell (x-y direction) and l_α is the length (z direction) and $f(\bar{r})$ is the integrand.

B. Partial Inductances and Coefficients of Potential

Starting with the integral equation (3), the first two terms (or vector potential terms) will be shown to correspond to partial inductances [1], [24]. Keeping in mind that the current density J is constant over each cell and $I_z = J_z a_{\text{cell}}$, where a_{cell} is the cross-sectional area of a cell, (3) becomes

$$\frac{j\omega\mu}{a_\alpha} I_z \int_{v_{\alpha'}} G(\bar{r},\bar{r}')\, dv_{\alpha'} + \frac{j\omega\mu}{a_\beta} I_z \int_{v_{\beta'}} G(\bar{r},\bar{r}')\, dv_{\beta'}. \quad (5)$$

Now, by applying (4), the vector potential terms in (5) become

$$\frac{j\omega\mu}{a_\alpha a_\alpha} I_z \int_{v_{\alpha'}}\int_{v_\alpha} G(\bar{r},\bar{r}')\, dv_\alpha\, dv_{\alpha'} + \frac{j\omega\mu}{a_\beta a_\alpha} I_z \int_{v_{\beta'}}\int_{v_\alpha} G(\bar{r},\bar{r}')\, dv_\alpha\, dv_{\beta'}. \quad (6)$$

From [24], the partial inductance between cells α and β is defined as

$$Lp_{\alpha\beta} = \frac{\mu}{4\pi}\frac{1}{a_\alpha a_\beta}\int_{a_\alpha}\int_{a_\beta}\int_{l_\alpha}\int_{l_\beta} \frac{d\bar{l}_\beta \cdot d\bar{l}_\alpha}{R}\, da_\alpha\, da_\beta. \quad (7)$$

Using this definition and (2) for the Green's function, (6) can be rewritten as

$$j\omega Lp_{\alpha\alpha} I_\alpha + j\omega Lp_{\alpha\beta} I_\beta e^{-j\beta R_{\alpha\beta}} \quad (8)$$

where the first term is the partial self inductance of the cell α and the second term represents the inductive coupling to cell α from a current in cell β in Fig. 1. The delay between cells α and β are given by the phase term $e^{-j\beta R_{\alpha\beta}}$ where $R_{\alpha\beta}$ is the center-to-center distance between cells α and β. In general, given n cells, the inductive coupling term is

$$j\omega Lp_{ii} I_i + \sum_{j=1, i\neq j}^{n} j\omega Lp_{ij} I_j e^{-j\beta R_{ij}}. \quad (9)$$

In a similar manner, the coefficient of potential terms can be derived from the last three terms in (3). With the charge q is constant over each (3) becomes

$$\frac{q_\gamma}{\epsilon_0}\frac{\partial}{\partial z}\int_{S_{\gamma'}} G(\bar{r},\bar{r}')\, dS_{\gamma'} + \frac{q_\delta}{\epsilon_0}\frac{\partial}{\partial z}\int_{S_{\delta'}} G(\bar{r},\bar{r}')\, dS_{\delta'} + \frac{q_\zeta}{\epsilon_0}\frac{\partial}{\partial z}\int_{S_{\zeta'}} G(\bar{r},\bar{r}')\, dS_{\zeta'}. \quad (10)$$

Now, by applying (4), we get

$$\frac{q_\gamma}{\epsilon_0}\int_{v_\alpha}\frac{\partial}{\partial z}\int_{S_{\gamma'}} G(\bar{r},\bar{r}')\, dS_{\gamma'}\, dv_\alpha + \frac{q_\delta}{\epsilon_0}\int_{v_\alpha}\frac{\partial}{\partial z}\int_{S_{\delta'}} G(\bar{r},\bar{r}')\, dS_{\delta'}\, dv_\alpha + \frac{q_\zeta}{\epsilon_0}\int_{v_\alpha}\frac{\partial}{\partial z}\int_{S_{\zeta'}} G(\bar{r},\bar{r}')\, dS_{\zeta'}\, dv_\alpha. \quad (11)$$

The surface integral can be redefined at $F(z) = \int_S G(\bar{r},\bar{r}')\, dS$. With this, each term in (11) can be rewritten in terms of the $F(z)$

$$\frac{q_\gamma}{\epsilon_0}\int_{v_\alpha}\frac{\partial}{\partial z}F_\gamma(z)\, dv_\alpha + \frac{q_\delta}{\epsilon_0}\int_{v_\alpha}\frac{\partial}{\partial z}F_\delta(z)\, dv_\alpha + \frac{q_\zeta}{\epsilon_0}\int_{v_\alpha}\frac{\partial}{\partial z}F_\zeta(z)\, dv_\alpha. \quad (12)$$

Each volume integral can be broken into two integrals

$$\int_v \frac{\partial}{\partial z} F(z)\, dv = \int_a \int_z \frac{\partial}{\partial z} F(z)\, dz\, da. \tag{13}$$

The inner integral can be evaluated using a central difference approximation and the outer integral can be evaluated

$$\begin{aligned}\int_v \frac{\partial}{\partial z} F(z)\, dv &= \int_a \left(F\left(z + \frac{\triangle z}{2}\right) - F\left(z - \frac{\triangle z}{2}\right)\right) da \\ &= a[F(z^+) - F(z^-)]\end{aligned} \tag{14}$$

where $z^+ = z + \frac{\triangle z}{2}$ and similarly $z^- = z - \frac{\triangle z}{2}$. With this result, (10) becomes

$$\begin{aligned}&\frac{q_\gamma}{\epsilon_0}\left[\int_{S_{\gamma'}} G(\bar{r}^+, \bar{r}')\, dS_{\gamma'} - \int_{S_{\gamma'}} G(\bar{r}^-, \bar{r}')\, dS_{\gamma'}\right] \\ &\quad + \frac{q_\delta}{\epsilon_0}\left[\int_{S_{\delta'}} G(\bar{r}^+, \bar{r}')\, dS_{\delta'} - \int_{S_{\delta'}} G(\bar{r}^-, \bar{r}')\, dS_{\delta'}\right] \\ &\quad + \frac{q_\zeta}{\epsilon_0}\left[\int_{S_{\zeta'}} G(\bar{r}^+, \bar{r}')\, dS_{\zeta'} - \int_{S_{\zeta'}} G(\bar{r}^-, \bar{r}')\, dS_{\zeta'}\right].\end{aligned} \tag{15}$$

The definition of normalized coefficient of potential is given in [2] with the Galerkin matching as

$$pp_{\alpha\gamma} = \frac{1}{a_\alpha a_\gamma} \frac{1}{4\pi\epsilon_0} \int_{S_\alpha} \int_{S_{\gamma'}} \frac{1}{R}\, dS_\alpha\, dS_{\gamma'} \tag{16}$$

where the total charge on cell γ is given by $Q_\gamma = q_\gamma a_\gamma$ where a_γ is the surface area of cell γ. With this relationship and the coefficient of potential definition in (16), each term in (15) can be rewritten. The delay between the general capacitive cell α and cells γ, δ, and ζ are given by the phase terms

$$\begin{aligned}&Q_\gamma\left[pp_\gamma{}^+ e^{-j\beta R^+_{\alpha\gamma}} - pp_\gamma{}^- e^{-j\beta R^-_{\alpha\gamma}}\right] \\ &\quad + Q_\delta\left[pp_\delta{}^+ e^{-j\beta R^+_{\alpha\delta}} - pp_\delta{}^- e^{-j\beta R^-_{\alpha\delta}}\right] \\ &\quad + Q_\zeta\left[pp_\zeta{}^+ e^{-j\beta R^+_{\alpha\zeta}} - pp_\zeta{}^- e^{-j\beta R^-_{\alpha\zeta}}\right]\end{aligned} \tag{17}$$

where $R^+_{\alpha\gamma} = |\bar{r}^+_\alpha - \bar{r}'_\gamma|$ and $R^-_{\alpha\gamma} = |\bar{r}^-_\alpha - \bar{r}'_\gamma|$. In addition, $pp_\gamma{}^+$ is defined as in (16) where $R = R^+ = |\bar{r}^+_\alpha - \bar{r}'_\gamma|$. The above partial inductances and the potential coefficients play a key role in the model improvement in the next section.

III. PEEC Model Improvements

PEEC models are implemented using partial inductances and coefficients of potential in [2], [24] and in the above derivation by (7) and (16). Here, both integrals are evaluated by analytically integrating the $\frac{1}{R}$ dependence of the Green's function over the appropriate cells. The allowable approaches are limited by the fact that we want to be able to use the technique in both the time as well as the frequency domain. We cannot include the phase term of the Green's function under the integrals since we also need to be able to evaluate them in the time domain. Hence, the integration of the phase term is approximated by the evaluation at the centroid of each cell. This has shown to provide very good answers in the active range of the frequency domain in comparison with other integral equation based methods. It is the purpose of this section to derive a new way of calculating the partial inductance and coefficient of potential terms for both the time and the frequency domain, which improves the PEEC model for higher frequencies.

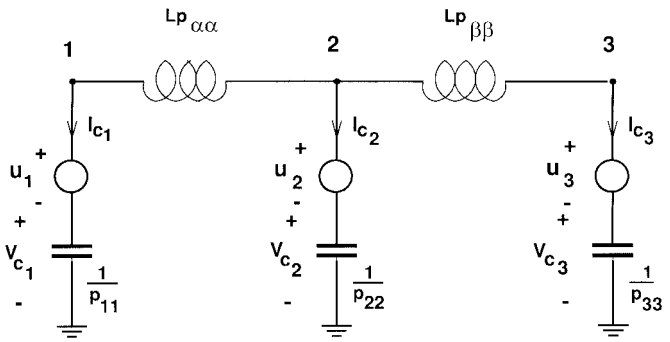

Fig. 2. PEEC model for conductor example.

A. Improvement Techniques

The partial inductance and coefficient of potential terms have been derived from the PEEC interpretation of the EFIE. Next, we develop an enhanced model which we call +PEEC for notational convenience.

A potential stabilization scheme for the time domain was proposed in [18] using PEEC. In [18], each inductive self cell was subdivided into two series inductances and a delay τ_s was introduced between these two inductances. It was shown analytically for a small model how the roots of the system could be moved from the right-half plane to the left-half plane by the proper assignment of τ_s. In this scheme, the delays were adjusted to obtain a stable model. We originally intended to prove that this split cell model also worked for larger problems. However, we found instead, that for more complex problems, this stabilization scheme was insufficient.

Both the MNA method and the loop or mesh-based MLA method can be used as a circuit formulations. Here, we use the MLA method. The PEEC model for the two-cell conductor example of Fig. 1 is shown in Fig. 2. It was shown in [8] that for this application, the MLA method is the most efficient implementation for PEEC in the frequency domain. It also can be related to the MoM impedance matrix for simple cases.

Again, we choose 20 cells/λ at $f_{\max}$ at the maximum frequency of interest $f_{\max}$. Assume that we would like to have a clean frequency response up to $50 f_{\max}$. This would require that we decrease the cell size by about a factor 50 in all directions. Such an increased range would comes at the high price of an extremely large number of unknowns and impossibly slow compute times. For clarity, we chose $f_{\max} = 20$ GHz in all our examples and we tried to obtain a clean model for the extended frequency range up to $f_e = 1000$ GHz. In the +PEEC formulation we try to obtain a sufficiently clean frequency response without increasing the number of unknowns. For this, we implement three changes in the PEEC which we are applying simultaneously to obtain the +PEEC model. Two improvement involve the partial inductances and coefficients of potential. Along with these model improvements, we made another change in the model through the introduction of damping resistors. This combined

model with all three improvements is referred to as R+PEEC. In this section, we show how these concepts are implemented and results are given in Section IV, which show how this stabilizes the PEEC models.

1) New Partial Inductance and Potential Coefficients: Our goal is to increase the accuracy of the phase behavior for the extended frequency range without introducing more unknowns. If we look at the two-cell example of Figs. 1 and 2, we can consider each cell at the detailed level. By subdividing each of these cells into a finite number of partitions, we can introduce a new way of computing the inductance term for each cell at the macromodel level. By using the relationship in (9) for this two-cell equation we have

$$\begin{aligned} &j\omega Lp_{11}I_1 + j\omega Lp_{12}I_2 e^{-j\beta R_{12}} \\ &j\omega Lp_{22}I_2 + j\omega Lp_{21}I_1 e^{-j\beta R_{21}}. \end{aligned} \tag{18}$$

We can now subdivide each of these cells into a finite number of partitions given by $\triangle = c/nf_e$ where c is the speed of light in free-space, $n = 1, 2, \cdots$, and f_e is given by the upper end of the extended frequency range. By choosing n appropriately, the smallest number of partitions for each geometry can be selected such that the problem is stable and the computational effort is minimized. Importantly, the unknown current for each cell is not further subdivided resulting in the same number of unknowns! This partitioning of each cell results in each partial inductance term consisting of a summation over all the partitions in each cell. For each cell, (7) becomes

$$\begin{aligned} Lp_{ij}^{+} = \frac{\mu}{4\pi}\frac{1}{a_i a_j}\sum_{k=1}^{M_i}\sum_{kk=1}^{N_i}\sum_{q=1}^{M_j}\sum_{qq=1}^{N_j} e^{-j\beta R_{k,kk,q,qq}} \\ \times \int_{a_k}\int_{l_{kk}}\int_{a_q}\int_{l_{qq}} \frac{d\bar{l}_{kk}\cdot d\bar{l}_{qq}}{R}\, dl_{qq}\, da_q\, dl_{kk}\, da_k \end{aligned} \tag{19}$$

where cell i is partitioned into M_i by N_i sections and cell j is partitioned into M_j by N_j sections. Cell i consists of a total of M_iN_i partitions and cell j consists of a total of M_jN_j partitions. The phase term is taken outside of the integral and is approximated by defining R as the distance between the centroid of partition k, kk and of partition q, qq.

Each partition now is treated the same as each cell. For example, where there was previously one calculation for a partial self inductance for cell i, now there are four sum over all M_iN_i partitions contained within cell i. For the mutual terms, the calculation is similar in that there are four sums, where two sums are over the partitions due to cell i and two sums are over the partitions due to cell j as is shown in (19).

The computation of the partial self- and partial mutual-inductance terms has increased to the extent that M_iN_i operations are required for each partial inductance term. However, due to the small subcell size, the analytical integration is computed only for the self-cell terms. For all mutual terms, the integral can be approximated by $\frac{1}{R}$ using the centroid to centroid distance of each partition within each cell. Although the computation of the partial inductance terms has changed considerably with this scheme, the unknowns are the same as before.

In a similar manner, the coefficient of potential cells γ, δ, and ζ in Fig. 1 can be partitioned into subcells. In general, for each pair of cells i and j, the coefficient of potential calculation with the delay term is replaced by

$$\begin{aligned} pp_{ij}^{+} = \frac{1}{4\pi\epsilon_0}\frac{1}{a_i a_j}\sum_{k=1}^{M_i}\sum_{kk=1}^{N_i}\sum_{q=1}^{M_j}\sum_{qq=1}^{N_j} e^{-j\beta R_{k,kk,q,qq}} \\ \times \int_{w_k}\int_{l_{kk}}\int_{w_q}\int_{l_{qq}} \frac{1}{R}\, dl_{qq}\, dw_q\, dl_{kk}\, dw_k \end{aligned} \tag{20}$$

where each partition has a width w and length l corresponding to the surface of each partition. Cell i is partitioned into M_i by N_i sections and cell j is partitioned into M_j by N_j sections. The phase term is again outside of the integral, but is approximated by defining R as the distance between the centroid of partition k, kk and of partition q, qq.

This technique can be applied in both the frequency as well as the time domain for both coefficient since the retardation terms in (19) and (20) are directly translated into equivalent time delays.

2) Damping Resistor: Realistic problems involve losses that can also be included in the PEEC model. As is evident in the results section, we were able to further extend the useful frequency range, by the addition of a damping resistor which addresses stability at the upper portion of the extended frequency range. The PEEC method is powerful because general circuit solutions can be easily be implemented to take account losses.

We added a damping resistor in parallel to the partial inductances as shown in Fig. 4. Since each loop current through the partial inductance is an unknown, by adding the parallel resistor we added one additional loop current for each existing unknown. The challenge is to implement this parallel resistance without changing the size of the matrix, i.e., the number of unknowns. The unknown loop current in cell α is given by I_α. This loop current can be written in terms of the currents through the inductor and resistor in loop α as $I_\alpha = I_{R_{\alpha\alpha}} + I_{Lp_{\alpha\alpha}}$. The parallel impedance is given by

$$\frac{sLp_{\alpha\alpha}R_{\alpha\alpha}}{sLp_{\alpha\alpha} + R}. \tag{21}$$

By using this parallel impedance, we do not introduce an additional unknown into the MLA matrix. In general, the *matrix stamp* is of the following form for a given current I_{Lk} going through the kkth partial inductance

Row	$\cdots$	I_{Lk}	$\cdots$	RHS
k	0	$\frac{\alpha_k}{s+\alpha_k}Lp_{kk}s$	0	0.

The *stamp* for the coupling of the current I_{Ln} into each of the other partial inductance terms is

Row	$\cdots$	I_{Ln}	$\cdots$	RHS
k	$\cdots$	$\frac{\alpha_n}{s+\alpha_n}\frac{\alpha_k}{s+\alpha_k}Lp_{nk}se^{-s\tau_{Lnk}}$	$\cdots$	0

where $\alpha_n = \frac{R_n}{Lp_{nn}}$ and $\alpha_k = \frac{R_k}{Lp_{kk}}$.

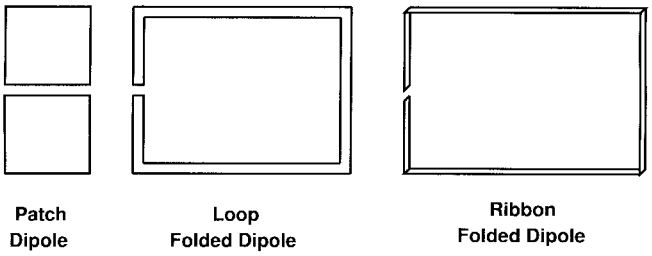

Fig. 3. Antenna geometries.

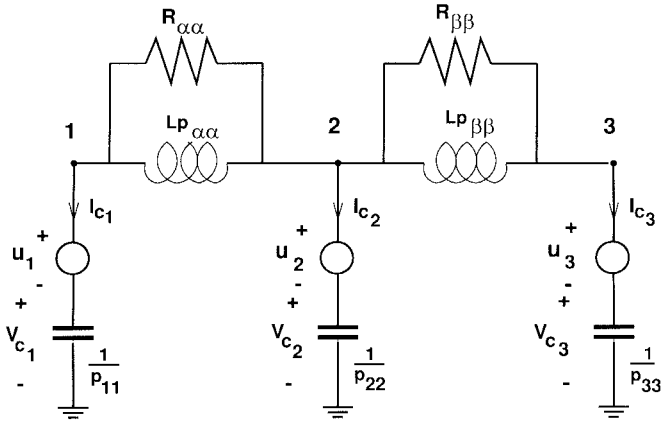

Fig. 4. PEEC model for conductor example with damping resistor.

The actual value of the damping resistor is calculated for each cell using the following:

$$R_{ii} = k\omega_{\max} Lp_{ii} \tag{22}$$

where $\omega_{\max} = 2\pi f_{\max}$, and $k = 10, \cdots 100$, depending on the problem. Using this equation for R, k may be adjusted such that R impacts the impedances at frequencies greater than $f_{\max}$, with only a small impact at frequencies lower than $f_{\max}$.

IV. Experimental Results

For our computer experiments, we used three different geometries, a patch antenna, and two folded dipole antennas shown in Fig. 3. They are representative of different classes of problems since the patch antenna is capacitive and the folded dipole antennas are inductive at low frequencies. As was stated in *Definition 1*, a negative real part of the input impedance indicates that the time solution may be unstable. In this section, we provide experimental evidence that implementing the partial inductance and coefficients of potential as outlined above results in an input impedance with a positive real part for a much larger frequency range. In addition, we were able to further extend the useful frequency range by the addition of the damping resistors.

The +PEEC and the R+PEEC improvements to the basic PEEC model in Section III are the result of extensive computer experiments. In this section, we give experimental evidence of the benefits of the model improvements. For all examples, the

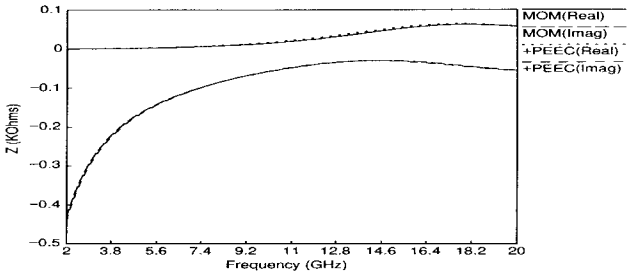

Fig. 5. MOM and +PEEC for a patch antenna.

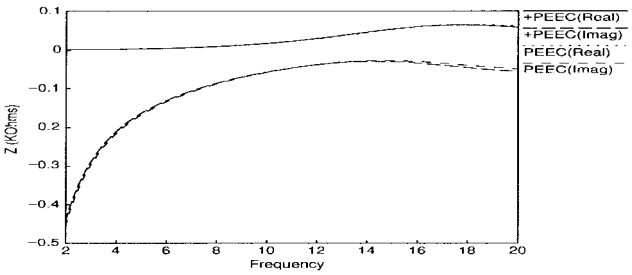

Fig. 6. PEEC and +PEEC for a patch antenna.

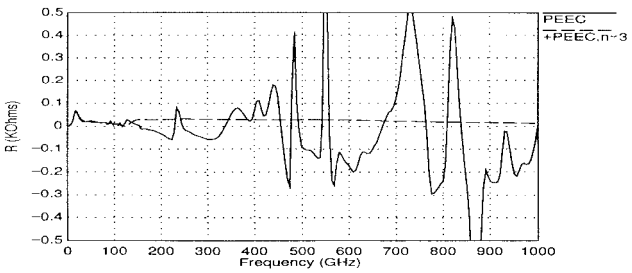

Fig. 7. Real input Z of PEEC and +PEEC for a patch antenna.

active frequency range approximately has $f_{\max} = 20$ GHz and the extended frequency is chosen to be $f_e = 1000$ GHz. We assume that the numerical integration method has enough numerical damping above f_e so that we do not need to be concerned with frequencies above f_e.

Our first comparison is for the *active* frequency range for a patch antenna where we show that the +PEEC model agrees very well with a carefully implemented MoM code [4]. The patch antenna, which is shown in Fig. 3, is center fed and has a length of 9 mm and a width of 4.5 mm. The real and imaginary input impedances are shown to be in close agreement in Fig. 5. Further, the PEEC and the +PEEC models are compared for the active region for the same example in Fig. 6 and again excellent agreement is shown.

The key issue of this paper is the *extended* frequency range. In order to show the impact of the model improvements, we give the input impedance up to f_e. Figs. 7 and 8 show the real and the imaginary input impedances for the patch antenna. The partitioning (+PEEC) significantly reduces the spurious resonances throughout the extended region and, even more important, the real part of the input impedance is positive for the entire extended frequency range.

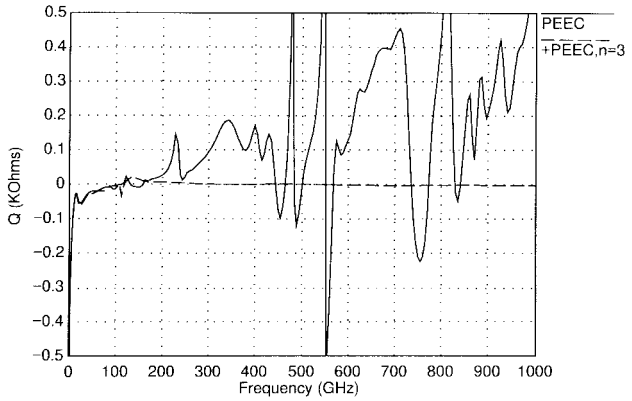

Fig. 8. Imaginary input Z of PEEC and +PEEC for a patch antenna.

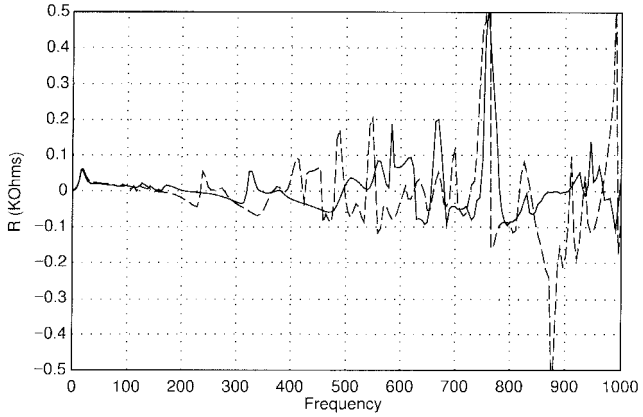

Fig. 9. Resonances using the PEEC model for a patch antenna.

The resonance behavior in the extended frequency response is very unpredictable for both MoM and PEEC techniques, depending on implementation details. Fig. 9 compares the real part for two close discretizations. We subdivided the structure with 20 cells/λ and 25 cells/λ at 20 GHz. This data shows the surprisingly strong dependence of the resonance behavior on the number of cells. These results clearly explain why the model time instability is a strong function of the discretization chosen.

Next we explore the effects of varying the subpartitioning in +PEEC. Recall that we can vary the partitioning using n in $\triangle = c/nf_e$. All the above results are based on $n = 3$. Fig. 10 shows the variation in the real part of the input impedance for $n = 1, 2, 3$ where $n = 1$ is the case without partitioning. This clearly illustrates the impact of this partitioning technique. For $n = 1$, the real input impedance turns negative at 450 GHz, for $n = 2$ it is positive up to 850 GHz, and for $n = 3$ it is positive up to 1000 GHz! In addition, the negative spike at 100–150 GHz are reduced by increasing the number of partitions used.

We show the impact of the damping resistor (R+PEEC) for the +PEEC model using $n = 3$ partitions. Results are given for the real part of the input impedance in Fig. 11. It is evident that the R helps to dampen the spike occurring between 100–150 GHz for all selected k values. The results

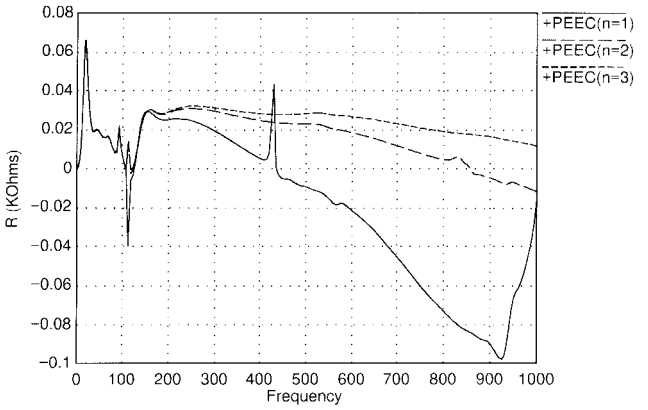

Fig. 10. Partitioning n for a patch antenna.

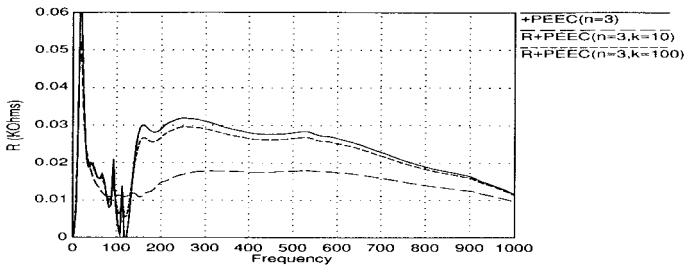

Fig. 11. Resistance for a patch antenna.

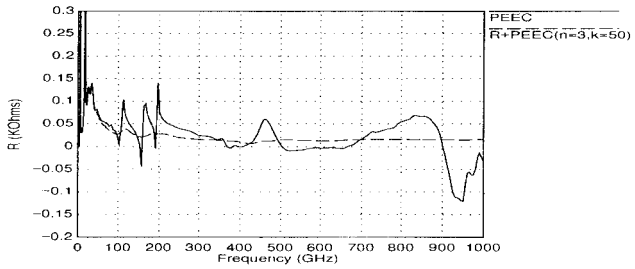

Fig. 12. PEEC and R+PEEC for a loop antenna.

with a damping resistor show show that positive real part can be obtained for entire extended frequency range for R+PEEC where $n = 3$ and $k = 100$! Referring back to Fig. 7, we see the remarkable difference between the new results and the original PEEC results without the stabilization scheme.

Fig. 3 shows one of the folded dipole antenna examples, which is referred to as a *loop*. This geometry has an edge-to-edge length of 9.9 mm, and an edge-to-edge width of 5.4 mm. All the zero thickness conductors have a width of 0.9 mm. The results for this geometry are shown in Fig. 12 for PEEC and $R+$ PEEC where we choose $n = 3$ and $k = 50$. Again, the stabilization scheme has eliminated the false resonances throughout the extended frequency range.

The second folded-dipole antenna example is referred to as a *ribbon*, which is also shown in Fig. 3. The zero thickness ribbon has an edge-to-edge length of 9 mm and an edge-to-edge width of 4.5 mm. Each conductor has a width of 0.9 mm. The number of partitions in this example are selected

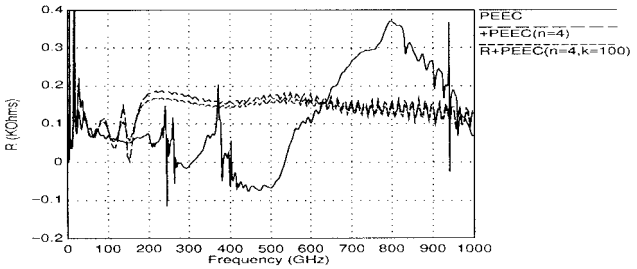

Fig. 13. PEEC, +PEEC and R+PEEC for a ribbon antenna.

to be $n = 4$ and $k = 100$ is used for the parallel resistor value. A comparison of PEEC, +PEEC, and R+PEEC for the real part of the input impedance is shown in Fig. 13. The results show that for this example the partitioning scheme (+PEEC) provides a stable solution, while the damping resistor (R+PEEC) provides additional smoothing for the extended frequency range. The comparison between the loop and the ribbon antenna results also shows that the small geometrical change of turning the zero thickness conductor results in a very large change in the extended frequency-domain responses.

V. Conclusion

The false resonances observed in this paper are key for the understanding of the the late-time instabilities that occur for integral-equation-type models. The process of eliminating these resonances is challenging. Our solution approach is assisted by the fact that the PEEC techniques transform the problem into the circuit domain. This allows the use circuit theory techniques and to introduce damping resistors into the circuit formulation without increasing the number of unknowns. The techniques are generally applicable to arbitrary geometries. We did not consider conductor series losses in this paper. This was done on purpose since the lossless case is a worst-case situation from a stability point of view. However, it is very desirable to include the series resistance in the actual model.

References

[1] C. R. Paul, *Introduction to Electromagnetic Compatibility*. New York: Wiley, 1992.
[2] A. E. Ruehli, "Equivalent circuit models for three dimensional multiconductor systems," *IEEE Trans. Microwave Theory Tech.*, vol. MTT-22, pp. 216–221, Mar. 1974.
[3] R. F. Harrington, *Field Computation by Moment Methods*. New York: Macmillan, 1968.
[4] B. J. Rubin and S. Daijavad, "Radiation and scattering from structures involving finite-size dielectric regions," *IEEE Trans. Antennas Propagat.*, vol. 38, pp. 1863–1873, Nov. 1990.
[5] A. E. Ruehli, J. Garrett, and C. R. Paul, "Circuit models for 3-D structures with incident fields," in *Proc. IEEE Int. Symp. Electromagn. Compat.*, Dallas, TX, Aug. 1993, pp. 28–31.
[6] A. E. Ruehli and H. Heeb, "Circuit models for three-dimensional geometries including dielectrics," *IEEE Trans. Microwave Theory Tech.*, vol. MTT-40, pp. 1507–1516, July 1992.
[7] J. E. Garrett and A. Ruehli, "PEEC-EFIE for modeling 3D geometries with lossy inhomogeneous dielectrics and incident fields," IBM Res. Rep. RC 19245 (#83733), IBM T. J. Watson Research Center, Yorktown Heights, NY, Oct. 1993.
[8] J. E. Garrett, A. Ruehli, and C. R. Paul, "Efficient frequency domain solutions for PEEC EFIE for modeling 3-D geometries," in *Proc. Int. Zurich Symp. Electromagn. Compat.*, Zurich, Switzerland, Mar. 1995, pp. 179–184.
[9] L. W. Nagel, "SPICE: A computer program to simulate semiconductor circuits," Elect. Res. Lab. Rep. ERL M520, Univ. California, Berkeley, May 1975.
[10] W. T. Weeks, A. J. Jimenez, G. W. Mahoney, D. Mehta, H. Quasemzadeh, and T. R. Scott, "Algorithms for ASTAP—A network analysis program," *IEEE Trans. Circuits Theory*, vol. CT-20, pp. 628–634, Nov. 1973.
[11] A. Tijhuis, *Electromagnetic Inverse Profiling: Theory and Numerical Implementation*. Utrecht, The Netherlands: VNU Sci. Press, 1987.
[12] B. P. Rynne and P. D. Smith, "Stability of time marching algorithms for electic field integral equations," *J. Electromagn. Waves Applicat.*, vol. JEWA-4, no. 12, pp. 1181–1205, Dec. 1990.
[13] E. K. Miller and J. A. Landt, "Direct time domain techniques for transient radiation and scattering from wires," *Proc. IEEE*, vol. 68, pp. 1396–1423, 1980.
[14] R. G. Martin, A. Salinas, and A. R. Bretones, "Time-domain integral equation methods for transient analysis," *IEEE Antennas Propagat. Mag.*, vol. 34, no. 3, pp. 15–22, June 1992.
[15] S. M. Rao, T. K. Sarkar, and S. A. Dianat, "The application of the conjugate gradient method to the solution of transient electromagnetic scattering from thin wires," *Radio Sci.*, pp. 1319–1326, Oct. 1984.
[16] A. Sadigh and E. Arvas, "Treating the instabilities in marching-on-in-time methods from a different perspective," *IEEE Trans. Antennas Propagat.*, vol. 41, pp. 1695–1702, Dec. 1993.
[17] R. S. Adve, T. K. Sarkar, O. M. Pereira-Filho, and S. M. Rao, "Extrapolation of time domain responses from three dimensional conducting objects utilizing the matrix pencil technique," *IEEE Trans. Antennas Propagat.*, to be published.
[18] A. E. Ruehli, U. Miekkala, and H. Heeb, "Stability of discretized partial element equivalent EFIE circuit models," *IEEE Trans. Antennas Propagat.*, vol. 43, pp. 553–559, June 1995.
[19] E. Chiprout and M. Nakhla, *Asymptotic Waveform Evaluation and Moment Matching for Interconnect Analysis*. Boston, MA: Kluwer, 1993.
[20] J. Cullum and A. Ruehli, "An extension of pseudospectral analysis for studying the stability and passivity of models of VLSI interconnects," IBM Res. Rep. RC 21016, IBM T. J. Watson Res. Ctr., Yorktown Heights, NY, Nov. 1997.
[21] N. Balabanin and T. Bickart, *Electrical Network Theory*. New York: Wiley, 1969.
[22] A. E. Ruehli, U. Miekkala, A. Bellen, and H. Heeb, "Stable time domain solutions for EMC problems using PEEC circuit models," in *Proc. IEEE Int. Symp. Electromagn. Compat.*, Chicage, IL, Aug. 1994, pp. 371–376.
[23] W. Pinello, A. Cangellaris, and A. Ruehli, "Hybrid electromagnetic modeling of noise interactions in packaged electronics based on the partial-element equivalent circuit formulation," *IEEE Trans. Microwave Theory Tech.*, vol. 45, pp. 1889–1896, Oct. 1997.
[24] A. E. Ruehli, "Inductance calculations in a complex integrated circuit environment," *IBM J. Res. Develop*, vol. 16, no. 5, pp. 470–481, Sept. 1972.

Jan E. Garrett (S'84–M'91) was born in Crestview, FL. She received the B.S. degree (with honors) in electrical engineering from the University of Florida, Gainesville, in 1986, the M.S. degree in electrical engineering from Purdue University, West Lafayette, IN, in 1987, and the Ph.D. degree from the University of Kentucky, Lexington, in electrical engineering in 1997.

Since 1989, Dr. Garrett has been with the Server Division of IBM. She has held various job positions in electromagnetic compatibility design and compliance in the area of high-frequency design tools and electromagnetic compatibility analysis and design. Presently, she is a Manager in Server Engineering Firmware Development. She has published several papers in the area of electromagnetic compatibility and modeling and she has given presentations on her work at several international conferences.

Dr. Garrett received an IBM outstanding Technical Achievement Award for her work on electromagnetic compatibility. She is a member of Tau Beta Pi and Eta Kappa Nu.

Albert E. Ruehli (M'65–SM'74–F'84) received the Ph.D. degree in electrical engineering in 1972 from the University of Vermont, Burlington.

He has worked at IBM on many different projects which include mathematical analysis, semiconductor circuits and devices, and as Manager of a VLSI design and CAD group. Since 1972, he has been at the IBM T. J. Watson Research Center, Yorktown Heights, NY, where he now is a Research Staff Member in the electromagnetic analysis group. He has given numerous talks at conference and universities and has organized many sessions. He has served in numerous capacities for the IEEE. He is the editor of *Circuit Analysis, Simulation and Design* (New York: North Holland, 1986, 1987) and is an author or coauthor of over 100 technical papers.

Dr. Ruehli received IBM Outstanding Contribution Awards in 1975, 1978, 1982, and 1995, and he received the Guillemin-Cauer Prize Award the IEEE Circuits and System Society for his work on waveform relaxation in 1982. He is a member of SIAM. In 1984 and 1985 he was Technical and General Chairman, respectively, of the ICCD International Conference. He has been a member of the IEEE ADCOM for the Circuit and System Society and an associate editor for the Transactions on CAD.

Clayton R. Paul (S'61–M'70–SM'79–F'87) was born in Macon, GA, on September 6, 1941. He received the B.S. degree, from The Citadel, Charleston, SC, in 1963, the M.S. degree, from Georgia Institute of Technology, Atlanta, GA, in 1964, and the Ph.D. degree, from Purdue University, West Lafayette, IN, in 1970, all in electrical engineering.

He is Emeritus Professor of electrical engineering at the University of Kentucky, Lexington, where he was a member of the faculty in the Department of Electrical Engineering for 27 years. He is currently the Sam Nunn Eminent Professor of Aerospace Systems Engineering in the Department of Electrical and Computer Engineering at Mercer University, Macon, GA. He is the author of 12 textbooks on electrical engineering subjects and has published over 200 technical papers, the majority of which are in his primary research area of electromagnetic compatibility of electronic systems. From 1970 to 1984, he conducted extensive research for the U.S. Air Force in modeling crosstalk in multiconductor transmission lines and printed circuit boards. From 1984 to 1990 he served as a consultant to the IBM corporation in the area of product electromagnetic compatibility design.

Dr. Paul is a member of Tau Beta Pi and Eta Kappa Nu.